Supplement of The Cryosphere, 16, 35–42, 2022
https://doi.org/10.5194/tc-16-35-2022-supplement

The Cryosphere Open Access

Supplement of

Brief communication: Increased glacier mass loss in the Russian High Arctic (2010–2017)

Christian Sommer et al.

Correspondence to: Christian Sommer (chris.sommer@fau.de)

Supplementary Data & Methods

1. TanDEM-X datasets

To derive surface elevation changes of glaciers on the Russian Arctic archipelagos, we use data from the TerraSAR-X add-on for Digital Elevation Measurement Mission (TanDEM-X), which is jointly operated by the German Aerospace Center (DLR) and Astrium Defense and Space. The TanDEM-X mission has been acquiring interferometric X-band data since 2010 (Krieger et al., 2007; Zink et al., 2016) and provides a complete global coverage. In this study, we compute digital elevation models from the TanDEM-X Co-registered Single look Slant range Complex (CoSSC) data product for the period 2010 to 2017. Whenever possible, TanDEM-X DEMs from winter 2010/11 and winter 2016/17 (Tab. S2) are selected to minimize potential biases of the measured elevation change due to varying depths of surface penetration of the X-band SAR or seasonal snow accumulation.

2. Calculation of glacier elevation and mass change

Interferometric elevation models are created and co-registered from TanDEM-X CoSSC data as described by (Braun et al., 2019; Seehaus et al., 2019). Differential interferograms are calculated, phase unwrapped and converted to elevation values based on a reference DEM. Unlike previous studies (Braun et al., 2019; Sommer et al., 2020; Farías-Barahona et al., 2020), we use the TanDEM-X Global DEM (German Aerospace Center (DLR), 2018) as a reference surface. Due to the unknown pixel acquisition dates, the Global DEM cannot be used directly to compute change rates. However, it provides a reliable reference surface without data voids for the interferometric processing of date-specific TanDEM-X acquisitions. To exclude ocean areas and water bodies from the processing, we use the OpenStreetMap (OSM) coastline and the HydroLAKES dataset (Messager et al., 2016). The OSM coastline was manually adjusted to improve the separation between ocean/sea ice and glacier areas and a small inverse buffer (100m) was applied to remove some biased pixels from the DEM co-registration. The 2010/11 TanDEM-X acquisitions are co-registered to the Global DEM on stable, ice-free areas (slope < 15°). The referenced DEMs are merged to create a 2010/11 elevation mosaic. Thereafter, the 2016/17 DEMs are co-registered and mosaiced based on the 2010/11 mosaic. In both cases, the co-registration is performed as an iterative process to remove vertical and horizontal shifts between the "raw" CoSSC DEMs and a reference surface. Initially, vertical biases are estimated (on stable areas) and corrected. Thereafter, horizontal shifts are minimized using an iterative approach of (Nuth and Kääb, 2011). Eventually, a second vertical correction is applied to reduce remaining offsets. Additionally, the acquisition dates of each raster cell are preserved alongside the elevation mosaics. Then, the mosaics are differenced and change rates are calculated using the respective dates of each individual track (Seehaus et al., 2019). Data voids in the resulting elevation change map are filled by applying an altitude dependent elevation change function on each archipelago, based on aggregated elevation change rates within 50m elevation bins (McNabb et al., 2019).

Eventually, the elevation change measurements (Fig. 2) are converted to geodetic mass changes ($\Delta M/\Delta t$) based on two density scenarios (ρ) with a) 850±60 kg m^{-3} as recommended by a study on alpine glaciers (Huss, 2013) and b) 900±60 kg m^{-3} as an approximation of the density of ice. Possible changes in the glacier ice density (e.g. firn compaction) are not considered, since we do not have any quantitative information on this for the Russian Arctic.

The resulting mass change does not include subaqueous ice volume change due to advance or retreat of the glacier termini because the geodetic approach can only resolve elevation change above sea-level.

Glacier areas are provided by the Randolph Glacier Inventory 6.0 (Pfeffer et al., 2014). For the Russian High Arctic, glacier outlines of the Randolph Glacier Inventory were mapped between 2000 and 2010 (Moholdt et al., 2012). Thus, the inventory represents the extent of glacierized areas a few years before the observation period of this study. A more recent glacier inventory (Rastner et al., 2017) based on optical and DEM data between 2013 and 2016 is available for Novaya Zemlya. The total glacierized areas of Novaya Zemlya of both inventories are similar, indicating no large-scale changes in glacier area between the inventories. In fact, the more recent inventory is slightly larger which is probably related to differences in the delineation of glacier outlines at high altitudes and the inclusion of very small glaciers (Rastner et al., 2017). Unfortunately, there are no other recent inventories available for glaciers on Franz Josef Land and Severnaya Zemlya. Therefore, we use the Randolph Glacier Inventory as it provides a homogenous dataset of glacier outlines for the entire Russian Arctic archipelagos. However, we made some manual adjustments to account for significant changes in glacier extents between the Randolph Glacier Inventory and the observation period of the TanDEM-X DEMs. The majority of adjustments is related to the retreat of marine-terminating glaciers on Novaya Zemlya and the surge of the Vavilov ice cap (Severnaya Zemlya).

3. Conversion of SAR signal penetration depths and correction of vertical elevation differences

For the elevation and mass change calculation of the Novaya Zemlya ice cap, we apply a vertical correction to account for differences in SAR signal penetration depths due to varying surface conditions of glacier areas which were only measured in winter 2010/11 and autumn 2016. The local vertical correction factor is based on an empirical linear relationship between SAR backscatter intensity and measured vertical offsets found on overlapping glacier areas. Eventually, the model is transferred to all glacier areas on Novaya Zemlya which were covered during September 2016 to derive the relative difference in signal penetration length (see chapter 2). Initially, the uncorrected glacier elevation ($\Delta h/\Delta t_{uncorr.}$) and mass change rate ($\Delta M/\Delta t_{uncorr.}$) is calculated for Novaya Zemlya. Thereafter, the estimated vertical offset is added to the September 2016 elevation values and the corrected elevation ($\Delta h/\Delta t_{corr.}$) and mass change rate ($\Delta M/\Delta t_{corr.}$) is calculated. Uncorrected and corrected glacier change results are stated in Table 1.

Due to the side-looking viewing geometry of the TanDEM-X SAR sensor, the length of SAR signal penetration (into the glacier) differs from the observed vertical elevation difference between September and winter acquisitions. The magnitude of the signal penetration lengths could be related either to a scattering layer below the actual glacier surface, e.g. a previously melted and refrozen late-summer ice layer, or a reflection due to power loss of the X-Band signal when travelling through the glacier volume (volume scattering). To account for both scenarios, two different approaches are applied to convert the observed vertical elevation offsets on overlapping glacier areas to signal penetration:

3.1. Trigonometric estimation of signal penetration

Using trigonometric functions, the length of signal penetration into the volume can be estimated from the local incidence angle, the surface slope and the measured absolute vertical elevation difference between September and winter 2016/17 according to Eq. 1.

$$l_p = \Delta h_{W-A} \times \frac{\cos(\alpha)}{\cos(\Theta_l)} \quad \text{Eq. 1}$$

Where l_p is the length of SAR signal penetration into the volume, $\Delta h_{W\text{-}A}$ the vertical height difference between winter and autumn (September) acquisition, α the glacier surface slope and Θ_l the respective local incidence angle.

3.2. Two-way power signal penetration

Using the two-way power penetration into infinitely deep uniform volumes, the vertical differences between heights of autumn (September) and winter DEM acquisitions $\Delta h_{W\text{-}A}$ can be converted to signal penetration into the glacier volume according to Eq. 2 following (Dall, 2007):

$$l_p = \frac{d_{p2} \times 2}{\cos(\Theta_v)} \; ; \; d_{p2} \approx \Delta h_{W-A} \quad \text{Eq. 2}$$

where l_p is the penetration length and Θ_v the refraction angle into the volume. dp_2 is the two-way power penetration and can be approximated as the vertical elevation bias $\Delta h_{W\text{-}A}$ for small penetration depths (Dall, 2007). To derive the refraction angle (Θ_v), Eq. 3 (Snell´s law) is applied:

$$\sin(\Theta_v) = n_1 \times \frac{\sin(\Theta_l)}{n_2} \quad \text{Eq. 3}$$

where Θ_l is the local incidence angle, *n1* the refractive index of air (1.000293) and *n2* the refractive index of glacier ice. For the permittivity of ice, various values have been reported in literature (Rasmussen, 1986; Dowdeswell and Evans, 2004). In general, the refractive index of ice increases with depths due to changes in density. Therefore, we refer to a detailed in-situ study on refraction measurements from the ice surface down to depths of 150 m in Antarctica (Kravchenko et al., 2004). For snow and ice layers close to the surface (0 to -40 m depth), they found values between ~1.3 and ~1.5 as index of refraction. Thus, we apply a refractive index of ice (*n2*) of 1.4 as the approximate permittivity of ice close to the glacier surface.

Eventually, the mean signal penetration length l_p of the two-way power penetration conversion is 5.4 m while the trigonometric estimate is 3.1 m. In general, both estimates are higher than the measured vertical elevation difference of overlapping glacier areas $\Delta h_{W\text{-}A}$ (2.13 m) due to the side-looking geometry of the TanDEM-X SAR sensor. However, the spatial distribution of penetration l_p and the derived linear regressions (see 2.1) are similar because both conversions are based on the measured vertical offset and local incidence angle. Therefore, when rearranging Eq. 1 and Eq. 2, the influence on the actual spatial vertical correction of glacier areas which were acquired during September 2016 is very small. The average vertical correction values for all September 2016 glacier areas are 2.29 m and 2.30 m, respectively. Eventually, the corrected elevation change rate of Novaya Zemlya ($\Delta h/\Delta t_{corr.}$) is less than 0.01 m a^{-1} more negative when using the two-way power penetration estimate and the geodetic mass change results calculated with both values are almost identical.

4. Uncertainty assessment of glacier mass change

The uncertainty analysis (Eq. 4) of the regional geodetic mass changes ($\delta_{\Delta M/\Delta t}$) considers uncertainties from the DEM differencing ($\delta_{\Delta h/\Delta t}$, including spatial autocorrelation, hypsometric gap-filling & SAR signal penetration), glacier outline errors (δ_S) and the volume to mass conversion with a constant density assumption (δ_p) (Braun et al., 2019).

$$\delta_{\Delta M/\Delta t} = \sqrt{\left(\frac{\Delta M}{\Delta t}\right)^2 \times \left\{\left(\frac{\delta_{\Delta h/\Delta t}}{\frac{\Delta h}{\Delta t}}\right)^2 + \left(\frac{\delta_S}{S}\right)^2 + \left(\frac{\delta_p}{p}\right)^2\right\}} \quad \text{Eq. 4}$$

$\Delta M/\Delta t$ denotes the mass change estimate, $\Delta h/\Delta t$ the (gap-filled) mean glacier elevation change rate, S the total glacierized area and p the density used in the volume to mass conversion.

To derive the relative vertical precision of the DEM difference ($\delta_{\Delta h/\Delta t}$), elevation changes outside glacier areas and water are aggregated in 5° slope bins ($\sigma_{\Delta h/\Delta t}$) and filtered (1-99% quantile) to account for the dependence between $\Delta h/\Delta t$ precision and surface slope. Eventually, the vertical accuracy of the elevation change measurements on glacier areas is obtained by weighting the offsets of each slope bin by the slope distribution on glacierized areas ($\sigma_{\Delta h/\Delta t\ AW}$, Table S 1). To account for spatial autocorrelation, we use an average lag distance (d_l) of 318 m, derived from semivariograms of 100,000 random $\Delta h/\Delta t$ samples on stable areas, and Eq. 5 following (Rolstad et al., 2009):

$$S_{cor} = d_l^2 \times \pi$$

$$\delta_{\Delta h/\Delta t} = \sqrt{\frac{S_{cor}}{5 \times S_G}} \times \sigma_{\Delta h/\Delta t\ AW} + s_{pen} \quad for\ S_G > S_{cor} \quad \text{Eq. 5}$$

$$\delta_{\Delta h/\Delta t} = \sigma_{\Delta h/\Delta t\ AW} + s_{pen} \quad for\ S_G < S_{cor}$$

S_{cor} is the correlation area and S_G the glacier area multiplied by an empirical weighting factor of 5 (Rolstad et al., 2009).

To account for a potential bias in glacier surface elevation due to differences in SAR signal penetration between the acquisitions, we include a penetration offset factor (S_{pen}) within the elevation change uncertainty estimate ($\delta_{\Delta h/\Delta t}$). Therefore, we use the average vertical difference in surface elevation (~ 2 m) between September and winter acquisitions which was found on glacier areas above 400 m a.s.l. on Novaya Zemlya which were acquired in September and winter 2016/17 (see chapter 2.3 & 3). This penetration bias value is then weighted by the respective regional glacier area acquired in September 2016 (Franz Josef Land ~770 km², Novaya Zemlya ~7800 km²). For the corrected elevation change rate ($\Delta h/\Delta t_{corr.}$) of Novaya Zemlya (Table 1) we multiply the penetration offset (S_{pen}) of Novaya Zemlya by two. To consistently account for penetration differences in all subregions, we also apply S_{pen} to glacierized areas of Severnaya Zemlya. Since all DEMs covering the Severnaya Zemlya archipelago were acquired in the same season, we use a theoretical penetration difference of 1 m on areas above the regional median glacier elevation (438 m a.s.l.). For Severnaya Zemlya this error estimate can be seen as an upper bound because all DEMs were acquired under similar surface conditions and show no major differences in backscatter intensities (Fig. S1c).

Biases due to erroneous glacier areas (δ_S) are calculated with a scaling approach (Braun et al., 2019) based on a detailed evaluation of automatically and manually derived glacier outlines (Paul et al., 2013). Their comparison indicated a difference in area of 3%, corresponding to a perimeter to area ratio of 5.03 km^{-1} ($r_{P/S\ Paul\ et\ al.}$). To represent the different glacier geometries of the Russian Arctic archipelagos ($r_{P/S}$), δ_S is calculated according to Eq. 6:

$$\delta_S = \frac{r_{P/S}}{r_{P/S\ Paul\ et\ al.}} \times 0.03 \quad \text{Eq. 6}$$

The mass change uncertainty of the entire Russian Arctic is estimated as the quadrature sum of the regional errors of Franz Josef Land, Severnaya Zemlya and Novaya Zemlya (Dussaillant et al., 2019).

5. Creation of SAR backscatter and local incidence angle mosaics

Backscatter and SAR local incidence angle maps for each individual elevation model are derived from the TanDEM-X CoSSC data during the interferometric DEM creation. Thereafter, the horizontal shifts which are applied to the DEM raster during the co-registration are also applied to the backscatter and local incidence angle data. Eventually, the horizontally co-registered datasets are merged into mosaics of backscatter intensity and local incidence angles which are complementary to the elevation mosaics of the Russian Arctic archipelagos.

Table S 1 DEM corregistration statistics on non-glacierized areas for each subregion. $S_{glacier}$ refers to glacier areas with equal or less than 50° slope while $S_{no\text{-}ice}$ includes all areas (outside glaciers, ocean or lakes) with equal or less than 50° slope which were used during the corregistration. $\sigma_{\Delta h/\Delta t}$ and $\sigma_{\Delta h/\Delta t\ AW}$ are the total and glacier area-weighted standard deviations (2-98% quantile filtered) of $S_{no\text{-}ice}$ within 5° slope bins (methods section).

Region	$S_{glacier}$ <= 50° [km²]	$S_{no\text{-}ice}$ <= 50° [km²]	$\sigma_{\Delta h/\Delta t}$ [m a⁻¹]	$\sigma_{\Delta h/\Delta t\ AW}$ [m a⁻¹]
Franz Josef Land	12470	2565	0.279	0.135
Severnaya Zemlya	16444	15128	0.076	0.068
Novaya Zemlya	22073	19130	0.117	0.077

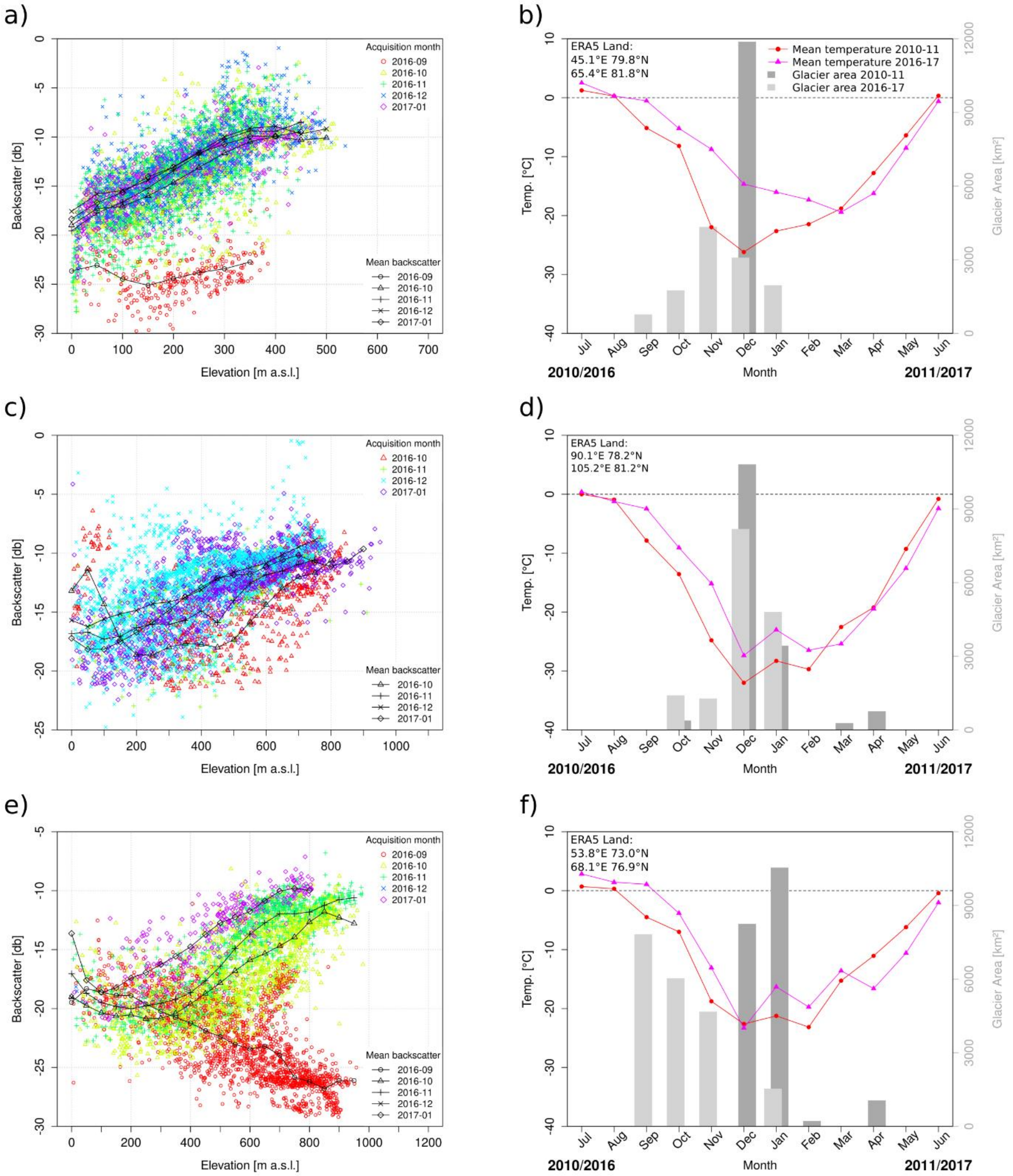

Figure S 1 Hypsometric distribution of backscatter intensity (random sample of 5000 cells) of different months of TanDEM-X acquisitions on Franz Josef Land a), Severnaya Zemlya c) and Novaya Zemlya e). Respective monthly mean skintemperatures of Franz Josef Land b), Severnaya Zemlya d) and Novaya Zemlya e) during years with TanDEM-X acquisitions were derived from ERA 5 Land reanalysis product *(Muñoz Sabater, 2019)***. Gray bars show the glacier area covered by TanDEM-X during winter 2010/11 and winter/autumn 2016/17. Climate data was extracted from ERA5 land grid cells within a bounding box around all glacierized areas of the respective archipelago. Ocean areas are not included and the corner coordinates are stated within the plots. (Generated using Copernicus Climate Change Service Information [2021])**

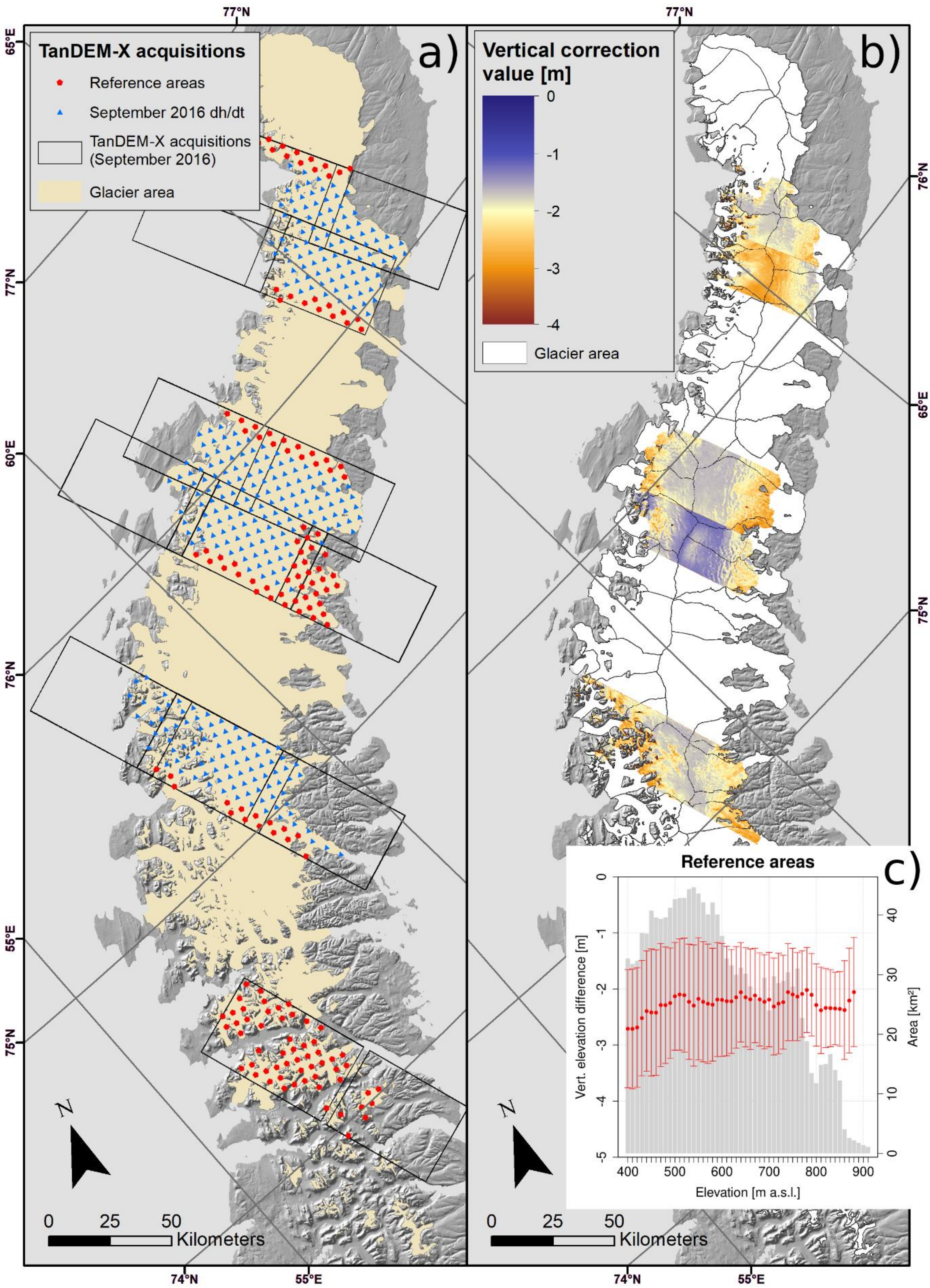

Figure S 2 a) Overview of temporal TanDEM-X coverage of Novaya Zemlya. Red dots indicate overlap areas which are covered by September and winter acquisitions 2016/17. Glacier areas which were only acquired during September 2016 are shown as blue triangles. b) Estimated vertical offset due to differences in SAR signal penetration between September and winter 2016/17 TanDEM-X DEMs. Vertical differences in the estimated correction field are caused by different local surface conditions and backscatter intensities of each September TanDEM-X acquisition. c) Observed vertical offsets of overlapping glacier areas (red dots in (a)).

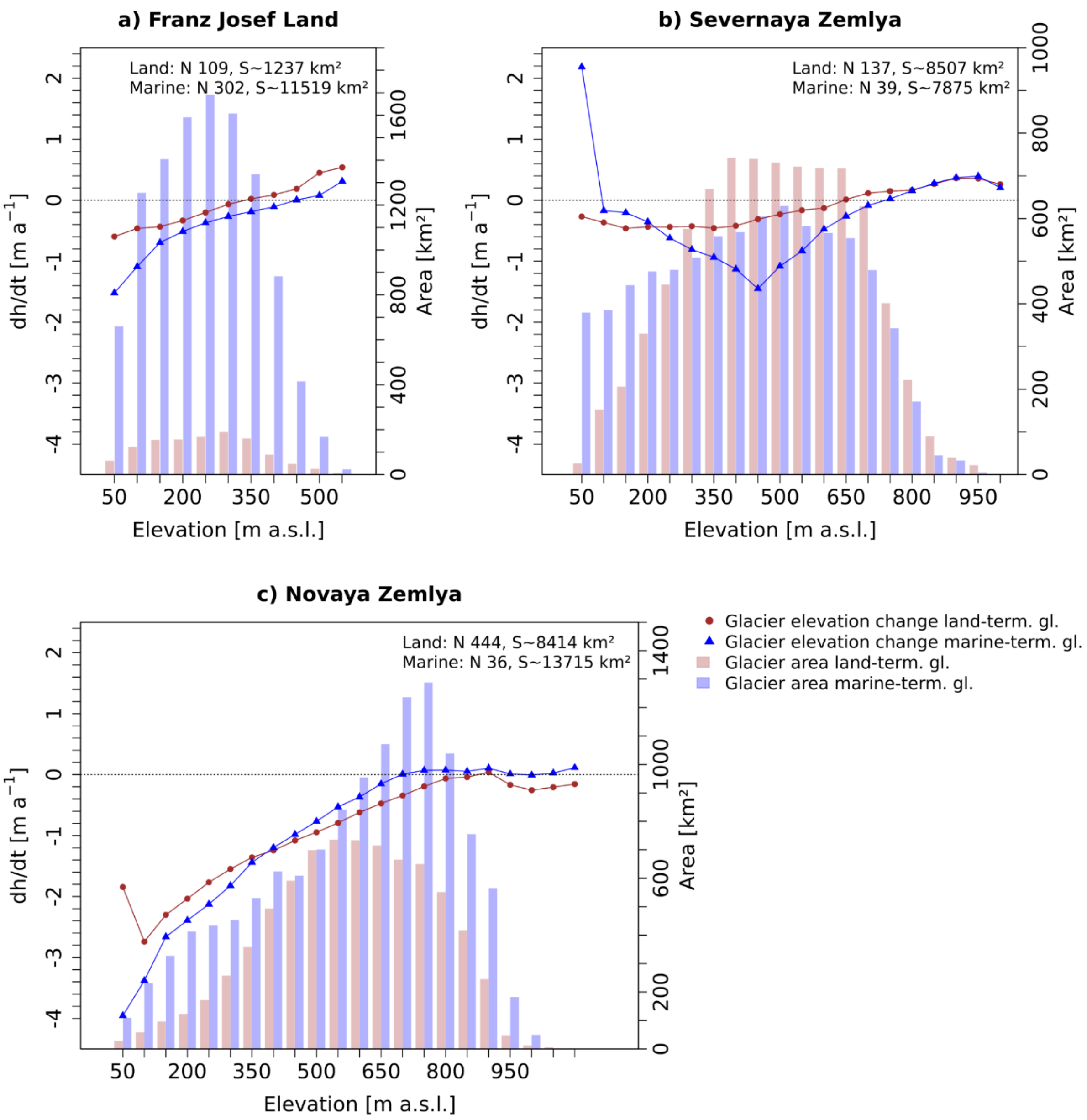

Figure S 3 Hypsometric distribution of elevation changes of land-terminating (brown dots) and marine-terminating (blue triangles) glaciers on Franz Josef Land (a), Severnaya Zemlya (b) and Novaya Zemlya (c). Respective glacier areas per elevation bin are shown as bars. The positive and less negative average elevation change rates below 450 m a.s.l. of marine-terminating glaciers on Severnaya Zemlya are caused by thickening in the ablation zones of some outlet glaciers (Academy of Sciences Ice Cap) and glacier surge activity (Vavilov Ice Cap). Elevation changes on Novaya Zemlya were corrected for SAR signal penetration. The less negative elevation change rate at lowest altitudes (< 50 m a.s.l.) of land-terminating glaciers on Novaya Zemlya is caused by glacier retreat during the observation period (i.e. areas which became ice-free) and temporal differences between the TanDEM-X observation period and the delineation of the glacier outlines.

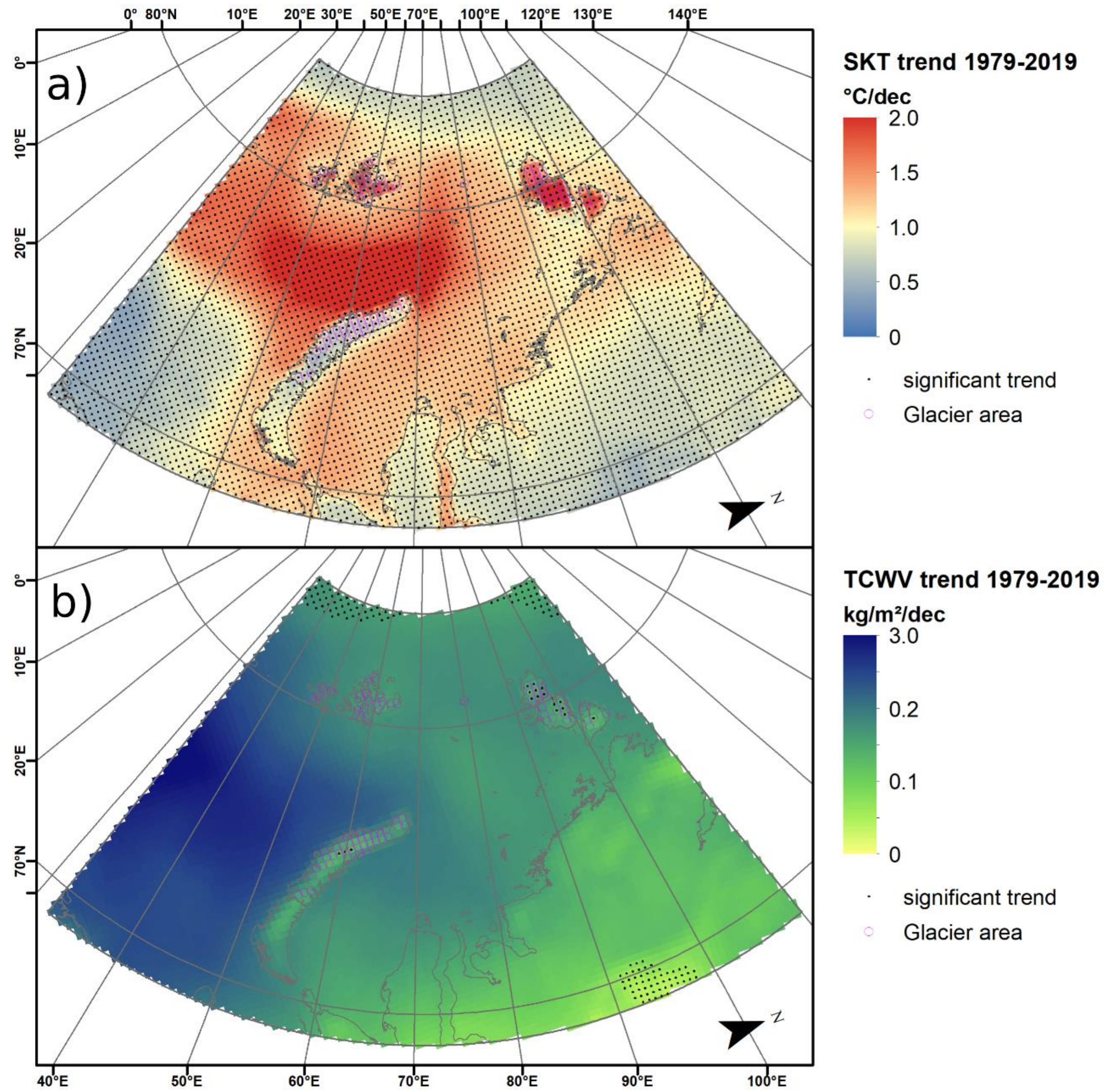

Figure S 4 a) Decadal trends in skintemperature (SKT) and b) total column water vapor (TCWV) between 1979 and 2019, derived from ERA5 reanalysis (Hersbach et al., 2020). Small gray dots show raster cells with significant trend ($P < 0.05$) while magenta circles represent cells with glacier areas.

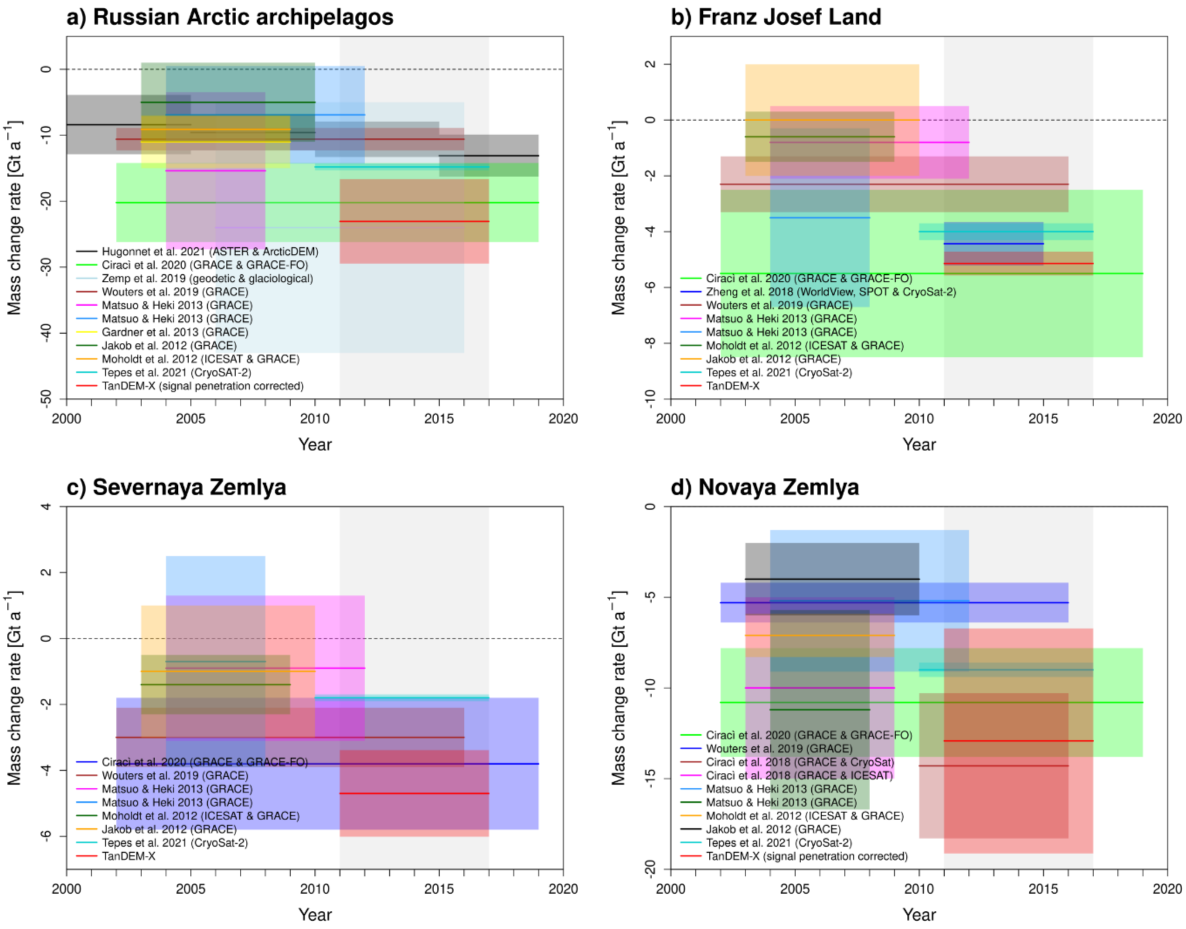

Figure S 5 Comparison of glacier mass change measurements in the entire Russian Arctic, Franz Josef Land, Severnaya Zemlya and Novaya Zemlya derived from gravimetry (GRACE), altimetry (ICESAT, CRYOSAT) and optical DEMs (ASTER, ArcticDEM). The method by Zemp et al. (2019) uses extrapolation based on glaciological and geodetic samples. For Novaya Zemlya the signal penetration corrected glacier mass change by TanDEM-X is shown.

Table S 2 Metadata of TanDEM-X acquisitions used to create the 2010/11 and 2016/17 DEM mosaics in this study. Active sensor indicates the transmitting and receiving sensor of the TanDEM-X satellite pair (TerraSAR-X & TanDEM-X) at the respective acquisition time. Number of scenes shows the number of acquisitions concatenated into one DEM strip.

***TSX-1=TerraSAR-X, TDX-1=TanDEM-X**

Date	*Start Time*	*Active sensor*	*Orbit Dir.*	*Relative orbit Number*	*Number of scenes*	*Effective Baseline [m]*	*Height Of Ambiguity [m]*	*Incidence Angle [°]*
12.12.2010	13:05:44	TSX-1	A	7	3	145.87	-46.24	40.69
12.12.2010	13:07:13	TSX-1	A	7	4	128.68	-52.24	40.67
13.12.2010	12:48:44	TSX-1	A	22	2	139.97	-44.87	38.49
13.12.2010	12:50:00	TSX-1	A	22	3	128.56	-52.78	40.68
14.12.2010	12:32:43	TSX-1	A	37	5	127.18	-52.5	40.68
15.12.2010	12:15:39	TSX-1	A	52	4	125.35	-53.44	40.67
16.12.2010	10:23:03	TSX-1	A	66	4	130.88	-51.26	40.68
16.12.2010	11:58:31	TSX-1	A	67	4	121.17	-51.39	38.49
16.12.2010	13:30:55	TSX-1	A	68	3	151.14	-44.97	40.65
17.12.2010	10:05:01	TSX-1	A	81	7	134.06	-52.32	40.68
17.12.2010	13:14:10	TSX-1	A	83	3	146.49	-46.15	40.67
17.12.2010	13:15:49	TSX-1	A	83	2	128.26	-52.93	40.68
18.12.2010	09:49:06	TSX-1	A	96	2	122.89	-51.28	38.47
18.12.2010	12:58:37	TSX-1	A	98	3	127.15	-53.03	40.66
19.12.2010	12:41:18	TSX-1	A	113	4	127.34	-52.48	40.67
20.12.2010	12:24:13	TSX-1	A	128	4	125.59	-53.23	40.69
21.12.2010	12:07:04	TSX-1	A	143	3	124.98	-53.75	40.66
21.12.2010	13:39:05	TSX-1	A	144	2	156.57	-47.19	42.72
22.12.2010	10:14:24	TSX-1	A	157	6	128.96	-51.47	40.67
22.12.2010	13:22:36	TDX-1	A	159	3	147.09	45.63	40.65
22.12.2010	13:24:29	TSX-1	A	159	2	127.78	-53.16	40.69
23.12.2010	13:05:40	TSX-1	A	7	3	138.7	-45.29	38.48
23.12.2010	13:07:13	TSX-1	A	7	4	121.33	-51.86	38.5
25.12.2010	12:32:44	TSX-1	A	37	5	119.71	-51.71	38.49
26.12.2010	12:15:40	TSX-1	A	52	3	117.53	-52.94	38.5
27.12.2010	10:23:14	TSX-1	A	66	1	122.59	-51.67	38.5
27.12.2010	11:58:31	TSX-1	A	67	3	121.03	-55.8	40.67
27.12.2010	13:31:04	TDX-1	A	68	3	148.47	48.73	42.66
28.12.2010	13:14:15	TSX-1	A	83	3	144.48	-49.99	42.69
28.12.2010	13:15:53	TSX-1	A	83	3	120.42	-52	38.52
29.12.2010	12:57:12	TSX-1	A	98	3	135.96	-46.18	38.5
29.12.2010	12:58:39	TSX-1	A	98	4	119.81	-52.08	38.5
30.12.2010	12:41:24	TSX-1	A	113	4	120	-52.07	38.52
31.12.2010	12:24:14	TSX-1	A	128	3	118.41	-52.52	38.51
01.01.2011	12:07:04	TSX-1	A	143	2	118.96	-52.98	38.49
02.01.2011	10:14:29	TSX-1	A	157	6	121.37	-50.6	38.52
02.01.2011	13:22:40	TSX-1	A	159	4	145.78	-49.19	42.68
03.01.2011	13:05:46	TDX-1	A	7	2	143.71	50.35	42.66
05.01.2011	12:31:36	TSX-1	A	37	2	134.71	-50.23	40.7
08.01.2011	13:14:05	TDX-1	A	83	3	137.17	45.56	38.48
09.01.2011	09:47:23	TSX-1	A	96	5	128.02	-52.06	38.45
09.01.2011	12:57:15	TDX-1	A	98	3	136.54	49.39	40.66

10.01.2011	12:40:09	TSX-1	A	113	2	132.06	-47.5	38.51
11.01.2011	12:23:03	TDX-1	A	128	2	133.57	50.76	40.63
14.01.2011	09:54:36	TSX-1	A	5	8	136.93	-55.33	40.42
16.01.2011	12:31:36	TDX-1	A	37	2	131.06	47.93	38.46
21.01.2011	12:40:09	TSX-1	A	113	2	135.07	-50.03	40.68
04.02.2011	13:22:28	TDX-1	A	159	3	134.88	46.23	38.47
20.02.2011	13:30:26	TSX-1	A	68	2	127.28	-50.71	38.48
02.04.2011	12:48:42	TSX-1	A	54	2	116.21	-58.24	40.67
06.04.2011	10:05:33	TSX-1	A	81	6	103.97	-59.4	38.47
12.04.2011	09:56:59	TSX-1	A	5	8	102.82	-61.6	38.5
27.04.2011	10:23:16	TSX-1	A	66	1	106.69	-66.88	42.62
11.10.2011	09:48:31	TSX-1	A	96	3	106.93	-63	40.66
30.03.2012	09:38:25	TSX-1	A	20	2	195.39	-34.8	39.36
07.09.2016	12:57:43	TDX-1	A	98	3	238.6	29.18	41.45
10.09.2016	12:07:34	TDX-1	A	143	4	188.73	33.99	39.34
12.09.2016	13:06:08	TSX-1	A	7	3	92.16	-70.26	39.4
13.09.2016	12:49:11	TSX-1	A	22	2	89.29	-72.61	39.39
14.09.2016	12:32:06	TSX-1	A	37	2	88.52	-73.05	39.4
17.09.2016	13:14:47	TSX-1	A	83	1	87.78	-67.95	37.15
27.09.2016	10:23:40	TSX-1	A	66	2	87.42	-78.31	41.51
28.09.2016	13:14:33	TSX-1	A	83	1	91.09	-66.15	37.14
28.09.2016	13:16:21	TSX-1	A	83	3	88.33	-78.23	41.48
29.09.2016	12:57:41	TSX-1	A	98	3	90.86	-71.17	39.39
30.09.2016	12:40:49	TSX-1	A	113	2	92.55	-74.9	41.48
30.09.2016	12:41:53	TSX-1	A	113	5	86.74	-79.22	41.5
01.10.2016	12:23:34	TSX-1	A	128	2	89.51	-72.44	39.37
07.10.2016	12:16:08	TSX-1	A	52	4	83.03	-77.55	39.39
08.10.2016	10:23:40	TSX-1	A	66	3	87.59	-79.13	41.5
08.10.2016	13:31:47	TSX-1	A	68	1	90.22	-66.27	37.19
10.10.2016	12:57:42	TSX-1	A	98	3	90.87	-71.16	39.39
14.10.2016	13:23:07	TSX-1	A	159	4	95.15	-72.6	41.46
15.10.2016	09:55:35	TSX-1	A	5	2	94.42	-77.26	41.47
16.10.2016	12:50:33	TSX-1	A	22	4	83.85	-76.78	39.39
20.10.2016	13:14:36	TSX-1	A	83	4	92.22	-69.85	39.35
20.10.2016	13:16:24	TSX-1	A	83	4	84.41	-76.24	39.39
21.10.2016	09:47:13	TSX-1	A	96	3	93.38	-77.22	41.46
21.10.2016	12:59:11	TSX-1	A	98	3	83.85	-76.97	39.4
22.10.2016	12:40:52	TSX-1	A	113	1	89.97	-71.79	39.38
22.10.2016	12:41:55	TSX-1	A	113	4	84.15	-76.13	39.42
24.10.2016	12:07:36	TSX-1	A	143	3	86.38	-80.02	41.48
26.10.2016	13:06:18	TSX-1	A	7	3	88.99	-67.16	37.19
29.10.2016	12:16:16	TSX-1	A	52	4	86.31	-80.01	41.48
30.10.2016	13:31:07	TSX-1	A	68	2	94.77	-69.02	39.4
02.11.2016	12:40:41	TSX-1	A	113	2	90.69	-71.39	39.36
06.11.2016	09:57:46	TSX-1	A	5	6	85.06	-76.39	39.37
07.11.2016	12:49:14	TSX-1	A	22	2	93.46	-74.39	41.48
07.11.2016	12:50:33	TSX-1	A	22	4	86.95	-79.16	41.51
08.11.2016	12:33:18	TSX-1	A	37	5	83.7	-76.37	39.38

10.11.2016	11:59:06	TSX-1	A	67	4	82.74	-77.55	39.41
11.11.2016	13:14:40	TSX-1	A	83	3	95.4	-72.72	41.49
16.11.2016	13:22:55	TSX-1	A	159	4	93.39	-68.97	39.39
16.11.2016	13:24:58	TSX-1	A	159	3	87.81	-78.91	41.49
27.11.2016	10:14:59	TSX-1	A	157	7	88.01	-78.72	41.46
04.12.2016	12:59:19	TSX-1	A	98	2	86.92	-79.77	41.46
06.12.2016	12:24:42	TSX-1	A	128	4	83.55	-76.76	39.4
09.12.2016	09:57:45	TSX-1	A	5	6	88.06	-79.73	41.44
09.12.2016	13:07:46	TSX-1	A	7	4	87.51	-78.83	41.48
15.12.2016	12:57:40	TSX-1	A	98	1	88.97	-67.77	37.17
15.12.2016	12:59:09	TSX-1	A	98	2	87.93	-78.94	41.48
20.12.2016	13:07:45	TSX-1	A	7	2	84.82	-76.28	39.37
21.12.2016	12:49:12	TSX-1	A	22	2	88.03	-68.1	37.13
25.12.2016	10:05:34	TSX-1	A	81	7	86.56	-76.33	39.41
30.12.2016	10:15:00	TSX-1	A	157	6	84.68	-75.79	39.42
30.12.2016	13:24:58	TSX-1	A	159	2	84.48	-76.88	39.4
02.01.2017	12:32:07	TSX-1	A	37	2	92.68	-74.84	41.49
02.01.2017	12:33:15	TSX-1	A	37	5	86.82	-79.1	41.5
04.01.2017	11:59:04	TSX-1	A	67	3	85.93	-80.69	41.49
04.01.2017	13:31:36	TSX-1	A	68	1	90.92	-66.24	37.18
05.01.2017	10:05:23	TSX-1	A	81	8	90.15	-79.37	41.48
19.01.2017	12:24:39	TSX-1	A	128	5	86.7	-79.54	41.48

References

Braun, M. H., Malz, P., Sommer, C., Farías-Barahona, D., Sauter, T., Casassa, G., Soruco, A., Skvarca, P., and Seehaus, T. C.: Constraining glacier elevation and mass changes in South America, Nature Clim Change, 9, 130–136, https://doi.org/10.1038/s41558-018-0375-7, 2019.

Ciracì, E., Velicogna, I. and Sutterley, T.: Mass Balance of Novaya Zemlya Archipelago, Russian High Arctic, Using Time-Variable Gravity from GRACE and Altimetry Data from ICESat and CryoSat-2, Remote Sensing, 10(11), 1817, doi:10.3390/rs10111817, 2018.

Ciracì, E., Velicogna, I. and Swenson, S.: Continuity of the Mass Loss of the World's Glaciers and Ice Caps From the GRACE and GRACE Follow-On Missions, Geophys. Res. Lett., 47(9), doi:10.1029/2019GL086926, 2020.

Copernicus Climate Change Service (C3S): ERA5: Fifth generation of ECMWF atmospheric reanalyses of the global climate. Copernicus Climate Change Service Climate Data Store (CDS), [online] Available from: https://cds.climate.copernicus.eu/cdsapp#!/home (Accessed 5 November 2020), 2017.

Dussaillant, I., Berthier, E., Brun, F., Masiokas, M., Hugonnet, R., Favier, V., Rabatel, A., Pitte, P., and Ruiz, L.: Two decades of glacier mass loss along the Andes, Nat. Geosci., 12, 802–808, https://doi.org/10.1038/s41561-019-0432-5, 2019.

Farías-Barahona, D., Sommer, C., Sauter, T., Bannister, D., Seehaus, T. C., Malz, P., Casassa, G., Mayewski, P. A., Turton, J. V., and Braun, M. H.: Detailed quantification of glacier elevation and mass changes in South Georgia, Environ. Res. Lett., 15, 034036, https://doi.org/10.1088/1748-9326/ab6b32, 2020.

Gardner, A. S., Moholdt, G., Cogley, J. G., Wouters, B., Arendt, A. A., Wahr, J., Berthier, E., Hock, R., Pfeffer, W. T., Kaser, G., Ligtenberg, S. R. M., Bolch, T., Sharp, M. J., Hagen, J. O., van den Broeke, M. R. and Paul, F.: A Reconciled Estimate of Glacier Contributions to Sea Level Rise: 2003 to 2009, Science, 340(6134), 852–857, doi:10.1126/science.1234532, 2013.

German Aerospace Center (DLR): TanDEM-X - Digital Elevation Model (DEM) - Global, 90m, https://doi.org/10.15489/JU28HC7PUI09, 2018.

Hersbach, H., Bell, B., Berrisford, P., Hirahara, S., Horányi, A., Muñoz-Sabater, J., Nicolas, J., Peubey, C., Radu, R., Schepers, D., Simmons, A., Soci, C., Abdalla, S., Abellan, X., Balsamo, G., Bechtold, P., Biavati, G., Bidlot, J., Bonavita, M., Chiara, G., Dahlgren, P., Dee, D., Diamantakis, M., Dragani, R., Flemming, J., Forbes, R., Fuentes, M., Geer, A., Haimberger, L., Healy, S., Hogan, R. J., Hólm, E., Janisková, M., Keeley, S., Laloyaux, P., Lopez, P., Lupu, C., Radnoti, G., Rosnay, P., Rozum, I., Vamborg, F., Villaume, S., and Thépaut, J.: The ERA5 global reanalysis, Q.J.R. Meteorol. Soc., 146, 1999–2049, https://doi.org/10.1002/qj.3803, 2020.

Hugonnet, R., McNabb, R., Berthier, E., Menounos, B., Nuth, C., Girod, L., Farinotti, D., Huss, M., Dussaillant, I., Brun, F., and Kääb, A.: Accelerated global glacier mass loss in the early twenty-first century, Nature, 592, 726–731, https://doi.org/10.1038/s41586-021-03436-z, 2021.

Huss, M.: Density assumptions for converting geodetic glacier volume change to mass change, The Cryosphere, 7, 877–887, https://doi.org/10.5194/tc-7-877-2013, 2013.

Jacob, T., Wahr, J., Pfeffer, W. T. and Swenson, S.: Recent contributions of glaciers and ice caps to sea level rise, Nature, 482(7386), 514–518, doi:10.1038/nature10847, 2012.

Krieger, G., Moreira, A., Fiedler, H., Hajnsek, I., Werner, M., Younis, M., and Zink, M.: TanDEM-X: A Satellite Formation for High-Resolution SAR Interferometry, IEEE Trans. Geosci. Remote Sensing, 45, 3317–3341, https://doi.org/10.1109/TGRS.2007.900693, 2007.

Matsuo, K. and Heki, K.: Current Ice Loss in Small Glacier Systems of the Arctic Islands (Iceland, Svalbard, and the Russian High Arctic) from Satellite Gravimetry, Terr. Atmos. Ocean. Sci., 24(4–1), 657, doi:10.3319/TAO.2013.02.22.01(TibXS), 2013.

McNabb, R., Nuth, C., Kääb, A., and Girod, L.: Sensitivity of glacier volume change estimation to DEM void interpolation, The Cryosphere, 13, 895–910, https://doi.org/10.5194/tc-13-895-2019, 2019.

Messager, M. L., Lehner, B., Grill, G., Nedeva, I., and Schmitt, O.: Estimating the volume and age of water stored in global lakes using a geo-statistical approach, Nat Commun, 7, 13603, https://doi.org/10.1038/ncomms13603, 2016.

Moholdt, G., Wouters, B. and Gardner, A. S.: Recent mass changes of glaciers in the Russian High Arctic: GLACIER MASS CHANGES, RUSSIAN ARCTIC, Geophys. Res. Lett., 39(10), n/a-n/a, doi:10.1029/2012GL051466, 2012.

Muñoz Sabater, J.: ERA5-Land monthly averaged data from 1981 to present. Copernicus Climate Change Service (C3S) Climate Data Store (CDS)., 2019.

Nuth, C. and Kääb, A.: Co-registration and bias corrections of satellite elevation data sets for quantifying glacier thickness change, The Cryosphere, 5, 271–290, https://doi.org/10.5194/tc-5-271-2011, 2011.

Paul, F., Barrand, N. E., Baumann, S., Berthier, E., Bolch, T., Casey, K., Frey, H., Joshi, S. P., Konovalov, V., Le Bris, R., Mölg, N., Nosenko, G., Nuth, C., Pope, A., Racoviteanu, A., Rastner, P., Raup, B., Scharrer, K., Steffen, S., and Winsvold, S.: On the accuracy of glacier outlines derived from remote-sensing data, Ann. Glaciol., 54, 171–182, https://doi.org/10.3189/2013AoG63A296, 2013.

Pfeffer, W. T., Arendt, A. A., Bliss, A., Bolch, T., Cogley, J. G., Gardner, A. S., Hagen, J.-O., Hock, R., Kaser, G., Kienholz, C., Miles, E. S., Moholdt, G., Mölg, N., Paul, F., Radić, V., Rastner, P., Raup, B. H., Rich, J., Sharp, M. J., and The Randolph Consortium: The Randolph Glacier Inventory: a globally complete inventory of glaciers, J. Glaciol., 60, 537–552, https://doi.org/10.3189/2014JoG13J176, 2014.

Rastner, P., Strozzi, T., and Paul, F.: Fusion of Multi-Source Satellite Data and DEMs to Create a New Glacier Inventory for Novaya Zemlya, Remote Sensing, 9, 1122, https://doi.org/10.3390/rs9111122, 2017.

Rolstad, C., Haug, T., and Denby, B.: Spatially integrated geodetic glacier mass balance and its uncertainty based on geostatistical analysis: application to the western Svartisen ice cap, Norway, J. Glaciol., 55, 666–680, https://doi.org/10.3189/002214309789470950, 2009.

Seehaus, T., Malz, P., Sommer, C., Lippl, S., Cochachin, A., and Braun, M.: Changes of the tropical glaciers throughout Peru between 2000 and 2016 – mass balance and area fluctuations, The Cryosphere, 13, 2537–2556, https://doi.org/10.5194/tc-13-2537-2019, 2019.

Sommer, C., Malz, P., Seehaus, T. C., Lippl, S., Zemp, M., and Braun, M. H.: Rapid glacier retreat and downwasting throughout the European Alps in the early 21st century, Nat Commun, 11, 3209, https://doi.org/10.1038/s41467-020-16818-0, 2020.

Tepes, P., Gourmelen, N., Nienow, P., Tsamados, M., Shepherd, A., and Weissgerber, F.: Changes in elevation and mass of Arctic glaciers and ice caps, 2010–2017, Remote Sensing of Environment, 261, 112481, https://doi.org/10.1016/j.rse.2021.112481, 2021.

Wouters, B., Gardner, A. S. and Moholdt, G.: Global Glacier Mass Loss During the GRACE Satellite Mission (2002-2016), Front. Earth Sci., 7, 96, doi:10.3389/feart.2019.00096, 2019.

Zemp, M., Huss, M., Thibert, E., Eckert, N., McNabb, R., Huber, J., Barandun, M., Machguth, H., Nussbaumer, S. U., Gärtner-Roer, I., Thomson, L., Paul, F., Maussion, F., Kutuzov, S. and Cogley, J. G.: Global glacier mass changes and their contributions to sea-level rise from 1961 to 2016, Nature, 568(7752), 382–386, doi:10.1038/s41586-019-1071-0, 2019.

Zheng, W., Pritchard, M. E., Willis, M. J., Tepes, P., Gourmelen, N., Benham, T. J. and Dowdeswell, J. A.: Accelerating glacier mass loss on Franz Josef Land, Russian Arctic, Remote Sensing of Environment, 211, 357–375, doi:10.1016/j.rse.2018.04.004, 2018.

Zink, M., Moreira, A., Bachmann, M., Brautigam, B., Fritz, T., Hajnsek, I., Krieger, G., and Wessel, B.: TanDEM-X mission status: The complete new topography of the Earth, in: 2016 IEEE International Geoscience and Remote Sensing Symposium (IGARSS), 2016 IEEE International Geoscience and Remote Sensing Symposium (IGARSS), Beijing, 317–320, https://doi.org/10.1109/IGARSS.2016.7729075, 2016.